HHS Public Access

Author manuscript

ACS Biomater Sci Eng. Author manuscript; available in PMC 2016 September 27.

Published in final edited form as:

ACS Biomater Sci Eng. 2015 ; 1(11): 1174–1182. doi:10.1021/acsbiomaterials.5b00319.

Endothelial Cellular Responses to Biodegradable Metal Zinc

Jun Ma[†,‡], **Nan Zhao**[†,‡], and **Donghui Zhu**[*,†,‡]

[†]Department of Chemical, Biological and Bio-Engineering, North Carolina Agricultural and Technical State University, 1601 East Market Street, Greensboro, North Carolina 27411, United States

[‡]NSF-ERC for Revolutionizing Metallic Biomaterial, North Carolina Agricultural and Technical State University, 1601 East Market Street, Greensboro, North Carolina 27411, United States

Abstract

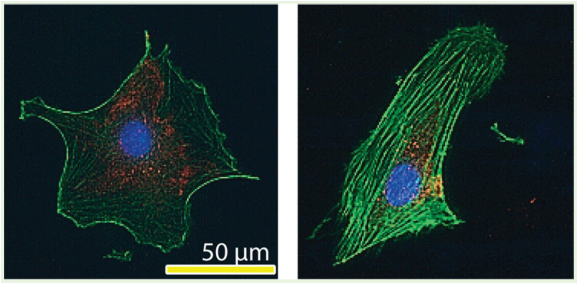

Biodegradable zinc (Zn) metals, a new generation of biomaterials, have attracted much attention due to their excellent biodegradability, bioabsorbability, and adaptability to tissue regeneration. Compared with magnesium (Mg) and iron (Fe), Zn exhibits better corrosion and mechanical behaviors in orthopedic and stent applications. After implantation, Zn containing material will slowly degrade, and Zn ions (Zn^{2+}) will be released to the surrounding tissue. For stent applications, the local Zn^{2+}concentration near endothelial tissue/cells could be high. However, it is unclear how endothelia will respond to such high concentrations of Zn^{2+}, which is pivotal to vascular remodeling and regeneration. Here, we evaluated the short-term cellular behaviors of primary human coronary artery endothelial cells (HCECs) exposed to a concentration gradient (0−140 μM) of extracellular Zn^{2+}. Zn^{2+} had an interesting biphasic effect on cell viability, proliferation, spreading, and migration. Generally, low concentrations of Zn^{2+} promoted viability, proliferation, adhesion, and migration, while high concentrations of Zn^{2+} had opposite effects. For gene expression profiles, the most affected functional genes were related to cell adhesion, cell injury, cell growth, angiogenesis, inflammation, vessel tone, and coagulation. These results provide helpful information and guidance for Zn-based alloy design as well as the controlled release of Zn^{2+}in stent and other related medical applications.

[*]**Corresponding Author** Phone: 336-285-3669. Fax: 336-334-7904. dzhu@ncat.edu.

The authors declare no competing financial interest.

Keywords

Zn; *stent*; *endothelial cell (EC)*; *cellular behaviors*; *biocompatibility*

INTRODUCTION

Biodegradable metals represent the next generation of promising biomaterials and scaffolds for orthopedic and cardiovascular implant applications. Their advantages over those of other permanent biomaterials include biodegradability, bioabsorbability, biocompatibility, and the ability to adapt to growth in young patients.[1] Among the three major biodegradable metals (Mg, Fe, and Zn), Mg-based alloys[2–9] and Fe-based alloys[10–14] have been the most widely explored. However, rapid corrosion associated with hydrogen evolution, rapidly accumulated degradation products, and loss of mechanical integrity make Mg alloys fail to support the local tissue healing process.[1] Moreover, some mechanical properties of Mg-based alloys, such as strength and ductility, are largely not satisfactory.[15] In contrast, the main shortcoming for Fe-based material is too slow degradation rate in physiological environments, thus causing problems similar to those found in permanent implants.[15]

However, Zn has been widely used as an alloying element in some Mg-based alloys. Previous studies showed that Zn could increase corrosion resistance,[16] decrease hydrogen evolution,[17] and improve strength and ductility simultaneously.[18] In addition, Zn is one of the most abundant essential elements in the human body, mostly in muscle and bone.[19] Zn plays important roles in the structure and function of over 300 enzymes and other macromolecules.[19] Therefore, it seems logical to explore Zn-based alloys as an alternative or perhaps a better choice based on their corrosion and mechanical and biocompatible properties.

Surprisingly, there were only limited studies on Zn-based alloys as implants reported in the literature before 2015. In one study, Zn was implanted into a Sprague–Dawley rat model to evaluate its suitability for stent application. Results revealed that the corrosion behavior was almost ideal and that within the first 4 months, Zn was degraded slowly, and the mechanical integrity was stably maintained. Then, corrosion was accelerated at 4.5 and 6 months.[20] In another study, Zn–Mg alloys with various Mg content (1%–3%) were evaluated for bone fixation. With 1% Mg, the Zn–Mg alloy had the maximum elongation and yield strength. All of the Zn–Mg alloys had lower corrosion resistance compared to that of pure Zn.[21] Recently, new studies on ultrapure Zn,[22] Zn–Mg–Sr,[23] and Zn-$_1$X (X = Mg, Ca, Sr)[24,25] were reported for their good mechanical properties, corrosion resistance, and biocompatibility. These studies indicated that Zn exhibited ideal corrosion behavior to match the process of wound healing and could be tailored to control corrosion behavior and mechanical properties for different medical applications.

After implantation, Zn^{2+} will be released from Zn-based alloys or other alloys with Zn to the surrounding extracellular spaces and further to the bloodstream. Zn^{2+} will have inevitable direct contact with vascular endothelial cells (ECs), and the local Zn concentration in the tissue could be high. Thus, the cellular responses to high extracellular Zn^{2+} are essential to the healing process as well as to evaluate the biocompatibility of these implants.

Furthermore, endothelialization, one of the important steps in arterial wound healing, determines the performance of stent materials containing Zn to a large extent.[26] However, unfortunately little is known about the interactions between ECs and Zn^{2+} at the cellular and molecular levels to date. Therefore, we studied the comprehensive short-term cellular responses of ECs under the influence of Zn^{2+}. Cell viability, cell proliferation, cell adhesion and spreading, cell migration, cytoskeleton reorganization, and gene expression profiles were explored.

EXPERIMENTAL SECTION

Zn^{2+} Solution Preparation

One millimolar $ZnCl_2$ solution was prepared by dissolving $ZnCl_2$ (Sigma-Aldrich, US) in deionized water. Then, the solution was filtered by a 0.22 μm filter (Fisher Scientific, US) and autoclaved (Harvey Sterile Max, Thermo Scientific, US). Before use, the solution was stored in a 4 °C refrigerator (Isotemp laboratory refrigerator, Fisher Scientific, US). The $ZnCl_2$ solution was diluted by endothelial cell medium (ECM, ScienCell, US) into solutions with different Zn^{2+} concentrations. The pH of different diluted solutions were measured by an Education pH meter (Fisher Scientific, US). Zn ion concentration range used in this study was 0–150 μM according to previous work[26] and our pilot experiment. The concentration of Zn, if over 150 μM, would be significantly toxic to cells (data not shown).

Cell Culture

Primary human coronary artery endothelial cells (HCECs) were purchased from ScienCell, US. The culture medium was ECM with 5% fetal bovine serum (FBS, ScienCell, US), 1% endothelial cell growth supplement (ECGS, ScienCell, US), and 1% penicillin/streptomycin solution (P/S, ScienCell, US). The cells were expanded in a 75 cm^2 culture flask (Falcon, BD Biosciences, US), and after the cells reached 90% confluence, they were washed with Dulbecco's phosphate-buffered saline (DPBS, Life technologies, US) and detached with trypsin/EDTA solution (Life technologies, US). Then, the cell solution was centrifuged (Sorvall Biofuge Stratos, Thermo Electro Corporation, US), and the supernatant was removed. The cell pellet was resuspended, and part of the cell solutions was mixed with 0.4% Trypan Blue Solution (Life technologies, US). Then, cell number was counted by a hemocytometer (Bright-Line, Hausser Scientific, US) under a microscope (EVOS FL Cell Imaging System, AMG, US). The cell solution was diluted into different concentrations for specific tests. Cells at passages of four to six were used in this study.

Cell Viability Test

The cell viability was detected by a 3-(4,5-dimethylthiazol-2-yl)-2,5-diphenyltetrazolium bromide assay (MTT assay, Vybrant, Life technologies, US). HCECs were seeded into a 96-well plate (Falcon, Corning, US) at the density of 5,000 cells/100 μL per well. After 24 h, the cell medium was replaced by fresh medium supplemented with different Zn^{2+} solutions. The plate was incubated at 37 °C, 5% CO_2, and 95% relative humidity for another 24 h. The medium was then replaced by 100 μL of fresh medium supplemented with 10 μL of 12 mM MTT stock solution and incubated for 4 h at 37 °C. Next, 100 μL SDS-HCl solution was added to each well and mixed thoroughly. The plate was incubated at 37 °C for another 4 h.

After that, the absorbance was measured by a microplate reader (Molecular Devices, US) at 570 nm. ECM with and without cells were used as positive control and negative control, respectively. Cell viability was calculated by the following formula:

$$\text{Cell viability} = \left(ABS_{\text{Sample}} - ABS_{\text{Negative}}\right) / \left(ABS_{\text{Positive}} - ABS_{\text{Negative}}\right)$$

Cell Proliferation Test

The cell proliferation was explored by a 5-bromo-2′-deoxyuridine kit (BrdU kit, Cell Signaling, US) according to the manufacturer's protocol. Briefly, the cells were seeded into a 96-well plate at the density of 5,000 cells/100 μL per well and allowed to attach for 24 h. After that, cell medium was replaced by 100 μL of fresh medium supplemented with different Zn^{2+} solutions and incubated for 24 h. Finally, the absorbance of the plate was measured by a microplate reader (Molecular Devices, US) at 450 nm. ECM with and without cells were used as positive and negative controls. The cell proliferation was determined as shown below:

$$\text{Cell proliferation} = \left(ABS_{\text{Sample}} - ABS_{\text{Negative}}\right) / \left(ABS_{\text{Positive}} - ABS_{\text{Negative}}\right)$$

Cell Adhesion Test and Centrifugation Assay

HCECs were mixed with Zn^{2+} solutions and seeded into a 24-well plate (Falcon, Corning, US). The final cell density was 50,000 cells/well. Cells were incubated at 37 °C, 5% CO_2, and 95% relative humidity for 2 or 6 h. Then, the cell medium was removed, and cells were washed by DPBS three times. Images of adhered cells were taken by a microscope (EVOS FL Cell Imaging System, AMG, US). The plate was sealed by self-sticking tape (Fisherbrand, Fisher Scientific, US). Then, the plate was put into the rotor inversely and centrifuged at 500 rpm for 5 min. Cells were washed by DPBS and fixed by 4% paraformaldehyde (Boston BioProducts, US). The images of adhered cells were taken by a microscope (EVOS FL Cell Imaging System, AMG, US) and analyzed by ImageJ (NIH, US). At least 10 different fields were used for calculating adhered cell density and cell retention ratio.

Cell Spreading Test

Cells were mixed with 60 μM or 140 μM Zn^{2+} solutions and seeded into 24-well plates at a density of 50,000 cells/well. At 0, 1, 2, 4, 6, and 8 h, cells were stained with calcein AM (Life technologies, US), and images were taken by a microscope (EVOS FL Cell Imaging System, AMG, US). Then, the images were analyzed by ImageJ (NIH, US). At least 10 different fields were used for measuring cell area and the perimeter.

Cell Migration Test

HCECs were seeded into a 24-well plate and after a monolayer was formed, the medium was removed. A P200 pipet tip (Fisher Scientific, US) was used to create a scratch in the monolayer. Cell debris and dead cells were washed away by DPBS. Then, cells were

incubated with different Zn^{2+} solutions at 37 °C, 5% CO_2, and 95% relative humidity for 6 h. The width of the scratch was measured at 0 and 6 h by ImageJ (NIH, US). At least 10 different points on the scratch were chosen for each concentration group to determine the width. Since cells migrated toward the scratch from two directions simultaneously, half of the width change was used in calculating cell migration rate. The average cell migration rate was calculated by the following formula:

$$\text{Cell migration rate} = 1/2\,(\text{width}_{0\text{h}} - \text{width}_{6\text{h}})\,/6$$

Cytoskeleton Staining and Cell Morphology

Cells were seeded on cover glasses (Fisherbrand, Fisher Scientific, US) in a 24-well plate at a density of 50,000 cells per well and incubated for 24 h. Then, the cell medium was replaced with 60 μM or 140 μM Zn^{2+} solutions and incubated for 24 h. After that, the cell medium was removed, and cells were washed with DPBS three times. Then, cells were fixed with 4% paraformaldehyde (Boston BioProducts, US) and permeabilized with 0.1% Triton X-100 (Fisher Scientific, US). After washing, cells were blocked by 5% bovine serum albumin (BSA, Fisher Scientific, US) solution for 1 h at room temperature. Then, the solution was removed, and the cells were washed with DPBS three times. Next, 2 μg/mL recombinant rabbit monoclonal vinculin antibody solution (Life technologies, US) was added and incubated for 2 h at room temperature. Then, the solution was removed, and cells were washed with DPBS for three times. After that, 4 μg/mL Alexa Fluoro 546 goat-antirabbit IgG solution (Life technologies, US) was added and incubated for 2 h at room temperature. Cells were washed with DPBS three times, and one drop of ActinGreen 488 ReadyProbes Reagent (Life technologies, US) was added to the cover glass. The plate was kept at room temperature in the dark for 30 min. After that, one drop of ProLong Gold Antifade Mountant with DAPI (Life technologies, US) was added to a clean glass slide (Thermo Scientific, US), and the cover glass was inversely placed on the glass slide. The cover glass was sealed by CoverGrip Covership Sealant (Biotium, US). The images of immunostaining and cell morphology were taken by a fluorescent microscope (EVOS FL Cell Imaging System, AMG, US) and were analyzed by ImageJ (NIH, US). At least 20 cells were used for the calculation of each concentration group. The aspect ratio and circularity were defined as shown below:

$$\text{Aspect ratio} = \text{major axis}/\text{minor axis}$$

$$\text{Circularity} = 4\pi \times \text{area}/\left(\text{perimeter}^2\right)$$

Gene Expression Profiles

HCECs were seeded into 60 mm Petri dishes (Primaria, Corning, US) and after a monolayer was formed, the cell medium was replaced by ECM supplemented with 60 μM or 140 μM Zn^{2+}. The ECM alone was used as a control group. The dishes were incubated for 24 h. Then, the cell culture medium was removed, and cells were washed with DPBS for three

times. The total RNA was isolated by RNeasy Mini Kit (Qiagen, US) according to the manufacturer's protocol. The purity and concentration of total RNA were determined by a spectrophotometer (Nanodrop 2000, US) at 230, 260, and 280 nm. The range of A_{260}/A_{280} was 2.03–2.06, and A_{260}/A_{230} was 2.14–2.26.

Next, 500 ng total RNA was transcripted reversely into cDNA by RT^2 First Strand Kit (Qiagen, US) following the manufacturer's protocol. RT-PCR was performed in CFX96 Touch RT-PCR Detection System (Bio-Rad, US) using Endothelial Cell Biology Array (Qiagen, US). The array plate includes 84 functional genes, 5 housekeeping genes, 1 genomic DNA control, 3 reverse transcription controls, and 3 positive PCR controls. Briefly, cDNA was mixed with RT^2 SYBR Green Master Mix (Qiagen, US) and RNase-free water. In the 96-well PCR array plate, 25 μL of the mixture was added to each well. After 10 min of incubation at 95 °C, cDNA was amplified according to the following steps: denaturing for 15 s at 95 °C, then annealing for 1 min at 60 °C, and 40 cycles were performed. After the amplification, *Ct* values were collected and analyzed by Bio-Rad CFX Manager 3.1 (Bio-Rad, US). The cutoff *Ct* value was 35. The ΔΔ*Ct* method was used to calculate fold changes of gene expression.

Statistical Studies

All of the data are presented as the mean ± SD. At least three replicates were used in every test for each concentration group. The statistical studies were performed with Student's *t* test (Prism 5, GraphPad Software, US), and $p < 0.05$ was considered as significant.

RESULTS

Zn^{2+} Induced Biphasic Changes on Cell Viability

Addition of Zn^{2+} induced interesting biphasic changes on cell viability as shown in Figure 1. A low concentration of 20 μM, Zn^{2+} significantly increased cell viability, and no adverse effects on cell viability was observed up to 100 μM. When the concentration reached above 100 μM, Zn^{2+} tended to inhibit cell viability significantly. No obvious changes in pH were observed in diluted Zn^{2+} solutions (data not shown).

Zn^{2+} Induced Biphasic Changes on Cell Proliferation

Similar to the cell viability test, a concentration gradient of Zn^{2+} was used, and Zn^{2+} induced biphasic changes on cell proliferation as well (Figure 2). At low concentrations up to 60 μM, Zn^{2+} promoted cell proliferation. When the concentration was above 80 μM, Zn^{2+} decreased the cell proliferation rate significantly.

Zn^{2+} Altered Cell Adhesion Property

To study the effect of Zn^{2+} on cell adhesion, a concentration gradient of Zn^{2+} was used at two different time points (Figure 3). At 2 h, both low and high concentrations of Zn^{2+} inhibited cell adhesion. While at 6 h, low concentrations (20–60 μM) of Zn^{2+} enhanced cell adhesion, and high concentrations (80–140 μM) of Zn^{2+} significantly inhibited cell adhesion. In addition, more cells were adhered at 6 h compared to that at 2 h (Figure 3a). Cell retention analysis revealed that at 6 h, less cells remained attached after centrifugation

at low concentrations (0–60 μM) of Zn^{2+}. In contrast, more cells remained attached when it was above 80 μM (Figure 3b).

Biphasic Effect of Zn^{2+} on Cell Spreading

Typical low (60 μM) and typical high (140 μM) concentrations of Zn^{2+} with a control were used to investigate cell spreading for a time course up to 8 h (Figure 4). At 60 μM Zn^{2+}, cell spreading was enhanced, and cells had a larger area (Figure 4a) and perimeter (Figure 4b) during the spreading process. In contrast, cell spreading was inhibited, and cells had a smaller area (Figure 4a) and perimeter (Figure 4b) at 140 μM Zn^{2+}. Also, all cell spreading progressed with time and reached a plateau phase around 8 h.

Biphasic Effect of Zn^{2+} on Cell Migration

Cells were exposed to a concentration gradient of Zn^{2+}. The relationship between cell migration rate and Zn^{2+} concentration was in a bell-like shape (Figure 5). Increasing Zn^{2+} concentration enhanced cell migration gradually but significantly and reached the highest value at 60 μM, and then started to decline. When the concentration of Zn^{2+} was over 100 μM, it significantly inhibited cell migration.

Effects of Zn^{2+} on Cytoskeletal Reorganization and Cell Morphology

Similarly, typical low (60 μM) and typical high (140 μM) concentrations of Zn^{2+} with a control were used to investigate the cell cytoskeletal reorganization and morphology. Typical representative images and corresponding quantitative analysis are shown in Figure 6. Zn^{2+} reorganized actin filaments and more actin stress fibers were observed with the presence of Zn^{2+} compared to that of the control (Figure 6a). Zn^{2+} also altered vinculin cellular localization (Figure 6a). More vinculins were gathered near the nuclear region when cells were treated with Zn^{2+}, while they were more evenly distributed throughout the entire cell in the control. In addition, 60 μM Zn^{2+} treatment enhanced the expression of actin filaments and vinculin significantly (Figure 6f and g). Cell morphology was largely dependent on Zn^{2+} concentration. In the control group, cells tended to be round in shape, while 60 μM Zn^{2+} treatment elongated the cells. Cells treated with 140 μM Zn^{2+} showed round but shrunken shape with much smaller cell area and perimeter (Figure 6b–e).

Zn^{2+} Altered Numerous Gene Expressions Differentially

Similar to previous experiments, typical low (60 μM) and typical high (140 μM) concentrations of Zn^{2+} with a control were used to investigate cell gene expression profiles. Functional genes affected most were related to cell adhesion, cell in jury, cell growth, angiogenesis, inflammation, vessel tone, and coagulation (Figure 7a and b). Genes *ACE*, *CCL2*, *EDN1*, *HMOX1*, *ICAM1*, *MMP1*, *NOS3*, *PDGFRA*, *PECAM1*, *PF4*, *PLAU*, *PTGIS*, *SELL*, *SERPINE1*, *TNFSF10*, and *VWF* were significantly altered by 60 μM or 140 μM Zn^{2+} (Figure 7c). Of these genes, *HMOX1*, *ICAM1*, *PTGIS*, and *SELL* had at least 2-fold changes in expression differentially ($p < 0.01$) (Figure 7d).

DISCUSSION

Despite the popularity of biodegradable metals including Zn-based or Zn as alloying element for biomedical applications, there are very limited studies on the effect of Zn on endothelial cells. It is still unknown how Zn^{2+}will affect the cells locally at cellular or molecular levels. Such information is urgently needed in order to have a better understanding and to design of future medical devices containing Zn. Therefore, we conducted a comprehensive evaluation of endothelial responses to Zn^{2+}followed by a gene expression profile check-up. The differential gene expression will provide useful genetic explanations on the phenotypes observed under the influence of Zn^{2+}.

We found that at low concentrations, Zn^{2+} had no adverse effects on cell viability, while Zn^{2+} decreased cell viability significantly if over 100 μM. Above 80 μM, Zn^{2+} significantly inhibited cell proliferation. Similar results were reported in a previous study that 15.38 μM Zn^{2+} significantly increased cell viability and proliferation of pig pulmonary artery endothelial cells, while at 153.8 μM, Zn^{2+} inhibited them significantly.[27] In another study, no obvious adverse effect of Zn^{2+} on cell viability was observed when below 600 μM for rat aorta endothelial cells.[28] Also, with the increase of concentration (0–100 μM), Zn^{2+} could induce bovine aorta endothelial cell death and increase the ratio of necrotic cells to total cells.[29] Our findings were generally consistent with these studies to a large extent, and different cell types, cell passages, serum usage, and other factors might count for the variations.

Next, we examine the effect of Zn^{2+}on endothelial cell mobility including adhesion, spreading, and migration. Cell adhesion is exerted by specialized subcellular contact sites of distinct structure and molecular composition (focal adhesions), formed by integrin associated with cytoskeleton. These sites serve as local anchors and link cells to the extracellular matrix.[30] Universal focal adhesion constituents include integrins, talin, vinculin, paxillin, c-reactive protein, zyxin, proto-oncogene tyrosine-protein kinase Src, and focal adhesion kinase.[31] In this study, four integrin-associated genes, *ITGA5, ITGAV, ITGB1*, and *ITGB3* were not significantly affected. However, the significant expression of actin and vinculin with 60 μM Zn^{2+} treatment could explain the observation that Zn^{2+} promoted cell adhesion at low concentrations.

Cell spreading is accompanied by changes in the structure and composition of the cytoskeleton.[32] In the process of cell spreading and locomotion, the assembly of early cell contacts to the extracellular matrix at the leading edge is driven by actin polymerization.[33] Besides the changes in cytoskeleton, cell spreading is also accompanied by cellular behaviors such as cell growth and differentiation.[32] A previous study showed that increasing spreading alone was sufficient to promote proliferation, while preventing cells from spreading had opposite effects. This finding was related to the internal mechanical tension developed within the actin cytoskeleton.[34] Endothelial cells proliferate more rapidly in growth factors containing medium as they become flatter. Growth stops when they take a rounded form, indicating the extent of spreading determines their ability to enter into the cell cycle.[35] In this study, we observed the overexpression of F-actin (polymerized actin) at 60 μM Zn^{2+} and decreased expression at 140 μM Zn^{2+}, which was consistent with the cell

spreading results. This finding on cell spreading was also consistent with that of cell proliferation.

Besides cell adhesion and spreading, cell migration is another important process in endothelial regeneration and vascular remodeling. For example, the rapid endothelialization on the stent surface is very critical in preventing intimal thickening and vascular thrombosis.[36] Usually, vascular injury triggers the proliferation and migration of endothelial cells, leading to re-endothelialization and repair of the injured vessel.[37] It is almost universal that cell migration involves four steps: protrusion of the leading edge, adhesion to the substratum, retraction of the rear, and deadhesion.[38] Therefore, optimal migration requires coordination between the formation of new adhesions at the cell front and subsequent release at the cell rear.[39] Cell migration and their speed depend on several factors, such as ligand levels, integrin levels, and integrin-ligand binding affinities.[40] In addition, increased integrin–ligand affinity could increase cell adhesion strength.[41] In this study, integrin-related genes were not significantly regulated by Zn^{2+}. However, a low concentration of Zn^{2+} (0–60 μM) did decrease the adhesion strength of endothelial cells to the tissue culture plate (Figure 3b), indicating the decreased affinity between integrins and ligands on the substrate. It might explain why Zn^{2+} at low concentrations significantly increased the cell migration rate. This was consistent with a common view that in order to remain motile, cells must maintain a low level of adhesion to ECM to allow traction, without attaching so firmly.[42]

Furthermore, we then investigated the effect of Zn^{2+}on cytoskeleton. The actin cytoskeleton plays important roles in forming and maintaining the shape and structure of cells. The reorganization of cytoskeleton alters cell shape and motility.[43] Several cellular processes, such as differentiation, growth, and apoptosis, are arbitrated by cell cytoskeletal organization and cell shape.[44] In this study, we observed reorganized stress fibers in cells treated with Zn^{2+}. The expression of stress fibers was enhanced at 60 μM but inhibited at 140 μM. These results were in line with cell proliferation. The actin cytoskeleton was also involved in the apoptosis process, and alterations of actin polymerization had profound effects not only on apoptosis but also on cellular morphology.[45] The apoptotic process is accompanied by sequential cell morphology change, such as membrane blebbing, cell fragmentation, and apoptotic body formation.[45,46] Therefore, both actin polymerization alterations and cell morphology changes could be used as indicators for cell apoptosis. Since depolymerization of F-actin occurs during apoptosis, our findings suggested that 60 μM Zn^{2+} could protect cells from apoptosis, while 140 μM Zn^{2+} was likely to induce apoptosis. This is in agreement with the notion that ECs treated by 140 μM Zn^{2+} tended to be more round shaped in cell morphology, an apoptotic indication.

Endothelial cells maintain elongated shape along the direction of blood flow when fluid shear stress remains high and unidirectional. Actin fibers are also reorganized to become aligned parallel to the direction of blood flow.[47] In the atherosclerotic lesions, endothelial cells are more round in shape, while endothelial cells in arterial regions, largely resistant to atherosclerosis, are more elongated in shape.[48] Elongated endothelial cells have been shown to have a lower inflammatory state with decreased intercellular adhesion molecule (ICAM) expression[49] and are more active in terms of migration[50,51] and proliferation.[50,52] Endothelial cells treated with 60 μM Zn^{2+} showed an elongated shape, in line with their

higher cell proliferation and migration rates. It might also suggest some antiatherosclerosis effects with low concentrations of Zn^{2+}.

Finally, to help explain the phenotype or cellular behaviors observed, we examined the gene expression profiles using an endothelial cell biology microarray. Of 16 significantly affected genes, *HMOX1, ICAM1, PTGIS*, and *SELL* were at least regulated by 2-fold. The *HMOX1* gene encodes heme oxygease-1 (HO-1), which catalyzes the degradation of free heme into biliverdin, Fe, and monoxide. HO-1 protects tissues during inflammatory stress and regulates inflammatory responses through the repression of proinflammatory genes.[53] One study showed that the function of HO-1 was mediated by the degradation products biliverdin, Fe, and carbon monoxide and that the three different degradation products could have beneficial effects alone or in combination.[54] Moreover, HO-1 is an inducible enzyme, and its expression is elicited by inflammatory stimulants, such as cytokines, heavy metals, and oxidants.[55] High concentration of Zn^{2+} at 140 μM significantly up-regulated *HMOX1*, suggesting that Zn^{2+} served as inflammatory simulants and induce inflammatory damage in this case. The beneficial effects of heme degradation products are likely to counteract the damage caused by stress and restore the hemostasis.[54]

Intercellular adhesion molecule-1 (ICAM-1), encoded by gene *ICAM1*, is expressed when endothelial cells are exposed to inflammation stimuli.[56] ICAM-1 regulates the physiological interaction between blood leukocytes and the blood vessel wall. ICAM-1 can be up-regulated to facilitate endothelia-leukocyte adhesion during the inflammation process.[57] We observed the significant up-regulation of the *ICAM1* gene at 140 μM Zn^{2+} and a slight down-regulation at 60 μM Zn^{2+}. It might explain why low concentrations of Zn^{2+} had beneficial effects on inflammation, while a high concentration of Zn^{2+} had adverse effects. This is consistent with a previous study[58] that the *ICAM1* gene was up-regulated in human umbilical vein endothelial cells (HUVEC) when treated with 50 μM Zn^{2+} for 4 h.

The *SELL* gene encodes L-selectin, which is responsible for the recruitment of circulating leukocytes to the inflammation sites of endothelium.[59] Low concentration of 60 μM Zn^{2+} significantly down-regulated the *SELL* gene, inhibiting the adhesion of leukocytes into endothelial cells. Prostaglandin-I synthase (PGIS), encoded by *PTGIS* gene, catalyzes prostaglandin H_2 (PGH_2) to prostacyclin (PGI_2). PGI_2 is a potent vasodilator and inhibitor of platelet aggregation.[60] Decreased PGIS was observed in lungs of patients with severe pulmonary hypertension.[61] PGI_2 deficiency could lead to the development of the thickening of the arterial wall in a mouse model.[62] In this study, *PTGIS* genes were up-regulated by Zn^{2+} at both 60 and 140 μM, but significance was observed only at 140 μM.

In cardiovascular stent applications, thrombogenicity, inflammation, and hyperplasia are also important aspects for biocompatibility evaluation of the stent materials. In this study, genes associated with blood coagulation including ANXA5, F2R, FAS, PF4, FAS, PLAT, PLAU, PROCR, SERPINE1, and *THBD* were examined. We found that Zn^{2+} at 60 μM significantly inhibited the expression of PF4, whereas it enhanced it at 140 μM. A previous study showed that both elevated *PF4* gene and platelet factor 4 (encoded by *PF4* gene) expression levels were observed in the peripheral blood cells in coronary artery disease.[63] Another important gene, *SERPINE1*, was significantly up-regulated by Zn^{2+} at 140 μM. Plasminogen activator

inhibitor-1 (PAI-1, encoded by *SERPINE1* gene) is a physiological inhibitor of tissue-type plasminogen activator and urokinase-type plasminogen activator, thus inhibiting the breakdown of clots. Increased expression of PAI-1 is a risk factor for thrombosis and atherosclerosis.[64] The gene expression profiles of these two genes might indicate that low concentration of Zn^{2+} was beneficial for coronary artery disease, while high concentration of Zn^{2+} might promote thrombosis formation. The *PF4* gene also plays an important role in inflammation. Released from locally activated platelets, platelet factor 4 can enter the vessel wall and promote vascular inflammation and atherogenesis.[65] Therefore, Zn^{2+} at 60 μM might help reduce the inflammation risk.

The expression of *HMOX1* and *NOS3* in HCECs was associated with the proliferation of smooth muscle cells (SMCs). *HMOX1* encodes HO-1 which catalyzes carbon monoxide. Carbon monoxide is one of the degradation products of free heme and has antiproliferative effects on SMCs.[54] The *NOS3* gene encodes nitric oxide synthase 3, responsible for synthesizing nitric oxide (NO). NO has been shown to inhibit platelet aggregation and SMC proliferation, thereby protecting against a later phase of atherogenesis.[66] High concentration of Zn^{2+} at 140 μM significantly up-regulated *HMOX1* while down-regulating *NOS3*. Therefore, it is hard to predict the overall effect of Zn^{2+} on hyperplasia (SMCs proliferation) from a gene expression perspective.

CONCLUSIONS

Cellular responses to Zn^{2+} were in a dose-dependent manner. At low concentrations, Zn^{2+} enhanced cell viability, proliferation, adhesion, spreading, migration, and F-actin and vinculin expression but decreased cell adhesion strength. In addition, a low concentration of Zn^{2+} altered cell morphology into an elongated shape. In contrast, high concentrations of Zn^{2+} had opposite effects. Extracellular Zn^{2+} concentration is tightly related to the implant degradation rate; therefore, a slow corrosion rate with controlled release of Zn^{2+} is desirable to keep a low concentration profile of Zn^{2+} in the local tissues, which is perhaps beneficial to endothelial cells.

ACKNOWLEDGMENTS

Research reported in this publication was supported by the National Institute of General Medical Sciences of the National Institutes of Health under Award Number SC3GM113762. The content is solely the responsibility of the authors and does not necessarily represent the official views of the National Institutes of Health. This work was also supported by National Science Foundation Engineering Research Center-Revolutionizing Metallic Biomaterials (ERC-RMB) at North Carolina A State University. We thank Dr. J. Waterman and Ms. D. Conklin for experimental training and help in facility usage.

REFERENCES

(1). Moravej M, Mantovani D. Biodegradable metals for cardiovascular stent application: interests and new opportunities. Int. J. Mol. Sci. 2011; 12(7):4250–4270. [PubMed: 21845076]

(2). Bosiers M, Investigators AI. AMS INSIGHT—absorbable metal stent implantation for treatment of below-the-knee critical limb ischemia: 6-month analysis. Cardiovascular and interventional radiology. 2009; 32(3):424–435. [PubMed: 19093148]

(3). Di Mario C, Griffiths H, Goktekin O, Peeters N, Verbist J, Bosiers M, Deloose K, Heublein B, ROHDE R, Kasese V. Drug–eluting bioabsorbable magnesium stent. Journal of interventional cardiology. 2004; 17(6):391–395. [PubMed: 15546291]

(4). Heublein B, Rohde R, Kaese V, Niemeyer M, Hartung W, Haverich A. Biocorrosion of magnesium alloys: a new principle in cardiovascular implant technology? Br. Heart J. 2003; 89(6):651–656.

(5). Peeters P, Bosiers M, Verbist J, Deloose K, Heublein B. Preliminary results after application of absorbable metal stents in patients with critical limb ischemia. Journal of Endovascular Therapy. 2005; 12(1):1–5. [PubMed: 15683259]

(6). Waksman R, Erbel R, Di Mario C, Bartunek J, de Bruyne B, Eberli FR, Erne P, Haude M, Horrigan M, Ilsley C. Early-and long-term intravascular ultrasound and angiographic findings after bioabsorbable magnesium stent implantation in human coronary arteries. JACC: Cardiovascular Interventions. 2009; 2(4):312–320. [PubMed: 19463443]

(7). Waksman R, Pakala R, Kuchulakanti PK, Baffour R, Hellinga D, Seabron R, Tio FO, Wittchow E, Hartwig S, Harder C. Safety and efficacy of bioabsorbable magnesium alloy stents in porcine coronary arteries. Catheterization and Cardiovascular Interventions. 2006; 68(4):607–617. [PubMed: 16969879]

(8). Zartner P, Buettner M, Singer H, Sigler M. First biodegradable metal stent in a child with congenital heart disease: evaluation of macro and histopathology. Catheterization and Cardiovascular Interventions. 2007; 69(3):443–446. [PubMed: 17295281]

(9). Zartner P, Cesnjevar R, Singer H, Weyand M. First successful implantation of a biodegradable metal stent into the left pulmonary artery of a preterm baby. Catheterization and Cardiovascular Interventions. 2005; 66(4):590–594. [PubMed: 16206223]

(10). Mueller PP, Arnold S, Badar M, Bormann D, Bach FW, Drynda A, Meyer-Lindenberg A, Hauser H, Peuster M. Histological and molecular evaluation of iron as degradable medical implant material in a murine animal model. J. Biomed. Mater. Res., Part A. 2012; 100(11):2881–2889.

(11). Peuster M, Hesse C, Schloo T, Fink C, Beerbaum P, von Schnakenburg C. Long-term biocompatibility of a corrodible peripheral iron stent in the porcine descending aorta. Biomaterials. 2006; 27(28):4955–4962. [PubMed: 16765434]

(12). Peuster M, Wohlsein P, Brügmann M, Ehlerding M, Seidler K, Fink C, Brauer H, Fischer A, Hausdorf G. A novel approach to temporary stenting: degradable cardiovascular stents produced from corrodible metal—results 6–18 months after implantation into New Zealand white rabbits. Br. Heart J. 2001; 86(5):563–569.

(13). Waksman R, Pakala R, Baffour R, Seabron R, Hellinga D, Tio FO. Short–term effects of biocorrodible iron stents in porcine coronary arteries. Journal of interventional cardiology. 2008; 21(1):15–20. [PubMed: 18086136]

(14). Wu C, Qiu H, Hu X, Ruan Y, Tian Y, Chu Y, Xu X, Xu L, Tang Y, Gao R. Short-term safety and efficacy of the biodegradable iron stent in mini-swine coronary arteries. Chinese medical journal. 2012; 126(24):4752–4757. [PubMed: 24342324]

(15). Schinhammer M, Hanzi ¨AC, Löffler JF, Uggowitzer PJ. Design strategy for biodegradable Fe-based alloys for medical applications. Acta Biomater. 2010; 6(5):1705–1713. [PubMed: 19654056]

(16). Hornberger H, Virtanen S, Boccaccini A. Biomedical coatings on magnesium alloys–a review. Acta Biomater. 2012; 8(7):2442–2455. [PubMed: 22510401]

(17). Zberg B, Uggowitzer PJ, Löffler JF. MgZnCa glasses without clinically observable hydrogen evolution for biodegradable implants. Nat. Mater. 2009; 8(11):887–891. [PubMed: 19783982]

(18). Chen Y, Xu Z, Smith C, Sankar J. Recent advances on the development of magnesium alloys for biodegradable implants. Acta Biomater. 2014; 10(11):4561–4573. [PubMed: 25034646]

(19). Tapiero H, Tew KD. Trace elements in human physiology and pathology: zinc and metallothioneins. Biomed. Pharmacother. 2003; 57(9):399–411. [PubMed: 14652165]

(20). Bowen PK, Drelich J, Goldman J. Zinc exhibits ideal physiological corrosion behavior for bioabsorbable stents. Adv. Mater. 2013; 25(18):2577–2582. [PubMed: 23495090]

(21). Vojtěch D, Kubásek J, Šerák J, Novák P. Mechanical and corrosion properties of newly developed biodegradable Zn-based alloys for bone fixation. Acta Biomater. 2011; 7(9):3515–3522. [PubMed: 21621017]

(22). Liu X, Sun J, Yang Y, Pu Z, Zheng Y. In vitro investigation of ultra-pure Zn and its mini-tube as potential bioabsorbable stent material. Mater. Lett. 2015 DOI: 10.1016/j.matlet.2015.06.107.

(23). Liu X, Sun J, Yang Y, Zhou F, Pu Z, Li L, Zheng Y. Microstructure, mechanical properties, in vitro degradation behavior and hemocompatibility of novel Zn-Mg-sr alloys as biodegradable metals. Mater. Lett. 2015 DOI: 10.1016/j.matlet.2015.07.151.

(24). Li H, Xie X, Zheng Y, Cong Y, Zhou F, Qiu K, Wang X, Chen S, Huang L, Tian L. Development of biodegradable Zn-1X binary alloys with nutrient alloying elements Mg, Ca and Sr. Sci. Rep. 2015; 5 10.1038/srep12190.

(25). Li H, Yang H, Zheng Y, Zhou F, Qiu K, Wang X. Design and characterizations of novel biodegradable ternary Zn-based alloys with IIA nutrient alloying elements Mg, Ca and Sr. Mater. Des. 2015; 83:95–102.

(26). Zhao N, Zhu D. Endothelial responses of magnesium and other alloying elements in magnesium-based stent materials. Metal-lomics. 2015; 7(1):118–128.

(27). Krones CJ, Klosterhalfen B, Butz N, Hoelzl F, Junge K, Stumpf M, Peiper C, Klinge U, Schumpelick V. Effect of zinc pretreatment on pulmonary endothelial cells in vitro and pulmonary function in a porcine model of endotoxemia. J. Surg. Res. 2005; 123(2):251–256. [PubMed: 15680386]

(28). Cortese MM, Suschek CV, Wetzel W, Kröncke K-D, Kolb-Bachofen V. Zinc protects endothelial cells from hydrogen peroxide via Nrf2-dependent stimulation of glutathione biosynthesis. Free Radical Biol. Med. 2008; 44(12):2002–2012. [PubMed: 18355458]

(29). Szuster-Ciesielska A, Stachura A, Słotwińska M, Kamińska T, Śniezko R, Paduch R, Abramczyk D, Filar J, Kandefer-Szerszen M. The inhibitory effect of zinc on cadmium-induced cell apoptosis and reactive oxygen species (ROS) production in cell cultures. Toxicology. 2000; 145(2):159–171. [PubMed: 10771141]

(30). Bershadsky A, Kozlov M, Geiger B. Adhesion-mediated mechanosensitivity: a time to experiment, and a time to theorize. Curr. Opin. Cell Biol. 2006; 18(5):472–481. [PubMed: 16930976]

(31). Li F, Zhang Y, Wu C. Integrin-linked kinase is localized to cell-matrix focal adhesions but not cell-cell adhesion sites and the focal adhesion localization of integrin-linked kinase is regulated by the PINCH-binding ANK repeats. Journal of Cell Science. 1999; 112(24):4589–4599. [PubMed: 10574708]

(32). Bhadriraju K, Hansen LK. Extracellular matrix-and cytoskeleton-dependent changes in cell shape and stiffness. Exp. Cell Res. 2002; 278(1):92–100. [PubMed: 12126961]

(33). Cavalcanti-Adam EA, Volberg T, Micoulet A, Kessler H, Geiger B, Spatz JP. Cell spreading and focal adhesion dynamics are regulated by spacing of integrin ligands. Biophys. J. 2007; 92(8): 2964–2974. [PubMed: 17277192]

(34). Roca-Cusachs P, Alcaraz J, Sunyer R, Samitier J, Farré R, Navajas D. Micropatterning of single endothelial cell shape reveals a tight coupling between nuclear volume in G1 and proliferation. Biophys. J. 2008; 94(12):4984–4995. [PubMed: 18326659]

(35). Re F, Zanetti A, Sironi M, Polentarutti N, Lanfrancone L, Dejana E, Colotta F. Inhibition of anchorage-dependent cell spreading triggers apoptosis in cultured human endothelial cells. J. Cell Biol. 1994; 127(2):537–546. [PubMed: 7523422]

(36). Van Belle E, Tio FO, Couffinhal T, Maillard L, Passeri J, Isner JM. Stent Endothelialization Time Course, Impact of Local Catheter Delivery, Feasibility of Recombinant Protein Administration, and Response to Cytokine Expedition. Circulation. 1997; 95(2):438–448. [PubMed: 9008462]

(37). McMullen ME, Bryant PW, Glembotski CC, Vincent PA, Pumiglia KM. Activation of p38 has opposing effects on the proliferation and migration of endothelial cells. J. Biol. Chem. 2005; 280(22):20995–21003. [PubMed: 15790570]

(38). Pollard TD, Borisy GG. Cellular motility driven by assembly and disassembly of actin filaments. Cell. 2003; 112(4):453–465. [PubMed: 12600310]

(39). Huttenlocher A, Ginsberg MH, Horwitz AF. Modulation of cell migration by integrin-mediated cytoskeletal linkages and ligand-binding affinity. J. Cell Biol. 1996; 134(6):1551–1562. [PubMed: 8830782]

(40). Palecek SP, Loftus JC, Ginsberg MH, Lauffenburger DA, Horwitz AF. Integrin-ligand binding properties govern cell migration speed through cell-substratum adhesiveness. Nature. 1997; 385(6616):537–540. [PubMed: 9020360]

(41). Xiao Y, Truskey GA. Effect of receptor-ligand affinity on the strength of endothelial cell adhesion. Biophys. J. 1996; 71(5):2869. [PubMed: 8913624]

(42). Messent AJ, Tuckwell DS, Knauper V, Humphries MJ, Murphy G, Gavrilovic J. Effects of collagenase-cleavage of type I collagen on alpha2beta1 integrin-mediated cell adhesion. Journal of cell science. 1998; 111(8):1127–1135. [PubMed: 9512508]

(43). Revenu C, Athman R, Robine S, Louvard D. The co-workers of actin filaments: from cell structures to signals. Nat. Rev. Mol. Cell Biol. 2004; 5(8):635–646. [PubMed: 15366707]

(44). Lipski AM, Pino CJ, Haselton FR, Chen I-W, Shastri VP. The effect of silica nanoparticle-modified surfaces on cell morphology, cytoskeletal organization and function. Biomaterials. 2008; 29(28):3836–3846. [PubMed: 18606447]

(45). Rao JY, Jin YS, Zheng Q, Cheng J, Tai J, Hemstreet GP. Alterations of the actin polymerization status as an apoptotic morphological effector in HL–60 cells. J. Cell. Biochem. 1999; 75(4):686–697. [PubMed: 10572251]

(46). Ndozangue-Touriguine O, Hamelin J, Bréard J. Cytoskeleton and apoptosis. Biochem. Pharmacol. 2008; 76(1):11–18. [PubMed: 18462707]

(47). Vartanian KB, Kirkpatrick SJ, Hanson SR, Hinds MT. Endothelial cell cytoskeletal alignment independent of fluid shear stress on micropatterned surfaces. Biochem. Biophys. Res. Commun. 2008; 371(4):787–792. [PubMed: 18471992]

(48). Gray BL, Lieu DK, Collins SD, Smith RL, Barakat AI. Microchannel platform for the study of endothelial cell shape and function. Biomed. Microdevices. 2002; 4(1):9–16.

(49). Wood JA, Shah NM, McKee CT, Hughbanks ML, Liliensiek SJ, Russell P, Murphy CJ. The role of substratum compliance of hydrogels on vascular endothelial cell behavior. Biomaterials. 2011; 32(22):5056–5064. [PubMed: 21501863]

(50). Schor AM, Schor SL, Allen TD. Effects of culture conditions on the proliferation, morphology and migration of bovine aortic endothelial cells. Journal of cell science. 1983; 62(1):267–285. [PubMed: 6619206]

(51). Madri JA, Pratt BM, Yannariello-Brown J. Matrix-driven cell size change modulates aortic endothelial cell proliferation and sheet migration. American journal of pathology. 1988; 132(1): 18. [PubMed: 3394798]

(52). Pratt B, Harris A, Morrow J, Madri J. Mechanisms of cytoskeletal regulation. Modulation of aortic endothelial cell spectrin by the extracellular matrix. American journal of pathology. 1984; 117(3):349. [PubMed: 6507585]

(53). True AL, Olive M, Boehm M, San H, Westrick RJ, Raghavachari N, Xu X, Lynn EG, Sack MN, Munson PJ. Heme oxygenase-1 deficiency accelerates formation of arterial thrombosis through oxidative damage to the endothelium, which is rescued by inhaled carbon monoxide. Circ. Res. 2007; 101(9):893–901. [PubMed: 17885218]

(54). Soares MP, Bach FH. Heme oxygenase-1: from biology to therapeutic potential. Trends Mol. Med. 2009; 15(2):50–58. [PubMed: 19162549]

(55). Duckers HJ, Boehm M, True AL, Yet S-F, San H, Park JL, Webb RC, Lee M-E, Nabel GJ, Nabel EG. Heme oxygenase-1 protects against vascular constriction and proliferation. Nat. Med. 2001; 7(6):693–698. [PubMed: 11385506]

(56). Marui N, Offermann M, Swerlick R, Kunsch C, Rosen C, Ahmad M, Alexander R, Medford R. Vascular cell adhesion molecule-1 (VCAM-1) gene transcription and expression are regulated through an antioxidant-sensitive mechanism in human vascular endothelial cells. J. Clin. Invest. 1993; 92(4):1866. [PubMed: 7691889]

(57). Kirkpatrick C, Wagner M, Kohler H, Bittinger F, Otto M, Klein C. The cell and molecular biological approach to biomaterial research: a perspective. J. Mater. Sci.: Mater. Med. 1997; 8(3): 131–141. [PubMed: 15348766]

(58). Martinotti S, Toniato E, Colagrande A, Alesse E, Alleva C, Screpanti I, Morrone S, Scarpa S, Frati L, Hayday AC. Heavy-metal modulation of the human intercellular adhesion molecule (ICAM-1) gene expression. Biochim. Biophys. Acta, Gene Struct. Expression. 1995; 1261(1): 107–114.

(59). Tedder T, Steeber D, Chen A, Engel P. The selectins: vascular adhesion molecules. FASEB J. 1995; 9(10):866–873. [PubMed: 7542213]

(60). Segurola RJ, Oluwole B, Mills I, Yokoyama C, Tanabe T, Kito H, Nakajima N, Sumpio BE. Cyclic strain is a weak inducer of prostacyclin synthase expression in bovine aortic endothelial cells. J. Surg. Res. 1997; 69(1):135–138. [PubMed: 9202659]

(61). Tuder RM, Cool CD, Geraci MW, Wang J, ABMAN SH, Wright L, Badesch D, Voelkel NF. Prostacyclin synthase expression is decreased in lungs from patients with severe pulmonary hypertension. Am. J. Respir. Crit. Care Med. 1999; 159(6):1925–1932. [PubMed: 10351941]

(62). Yokoyama C, Yabuki T, Shimonishi M, Wada M, Hatae T, Ohkawara S, Takeda J, Kinoshita T, Okabe M, Tanabe T. Prostacyclin-deficient mice develop ischemic renal disorders, including nephrosclerosis and renal infarction. Circulation. 2002; 106(18):2397–2403. [PubMed: 12403673]

(63). Ma J, Liew C-C. Gene profiling identifies secreted protein transcripts from peripheral blood cells in coronary artery disease. J. Mol. Cell. Cardiol. 2003; 35(8):993–998. [PubMed: 12878486]

(64). Mimuro J. [Type 1 plasminogen activator inhibitor: its role in biological reactions]. [Rinsho ketsueki] The Japanese journal of clinical hematology. 1991; 32(5):487–489. [PubMed: 1870265]

(65). Gawaz M, Langer H, May AE. Platelets in inflammation and atherogenesis. J. Clin. Invest. 2005; 115(12):3378. [PubMed: 16322783]

(66). Förstermann U, Sessa WC. Nitric oxide synthases: regulation and function. Eur. Heart J. 2012; 33(7):829–837. [PubMed: 21890489]

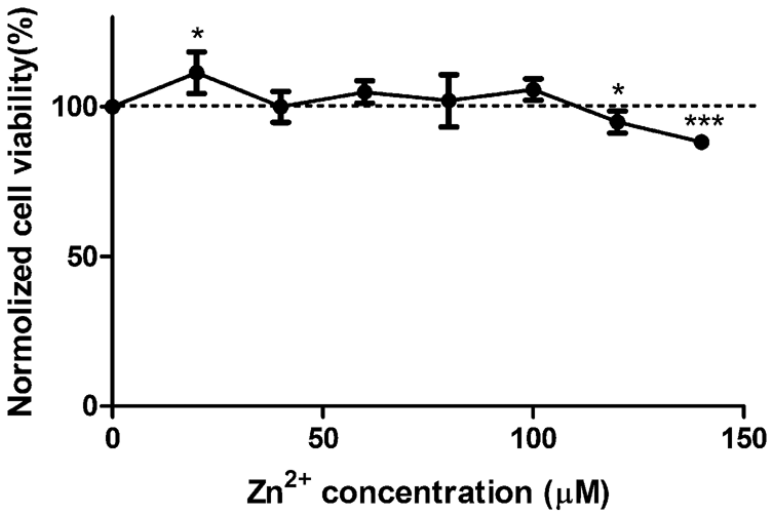

Figure 1.

Viability of cells treated with different concentrations of Zn^{2+}. ECs were seeded and allowed to attach for 24 h. Media were replaced with Zn^{2+} solutions, and cells were treated with Zn^{2+} for 24 h. Cell viability was detected by an MTT kit. Student's *t* test, * $p < 0.05$ and *** $p < 0.001$.

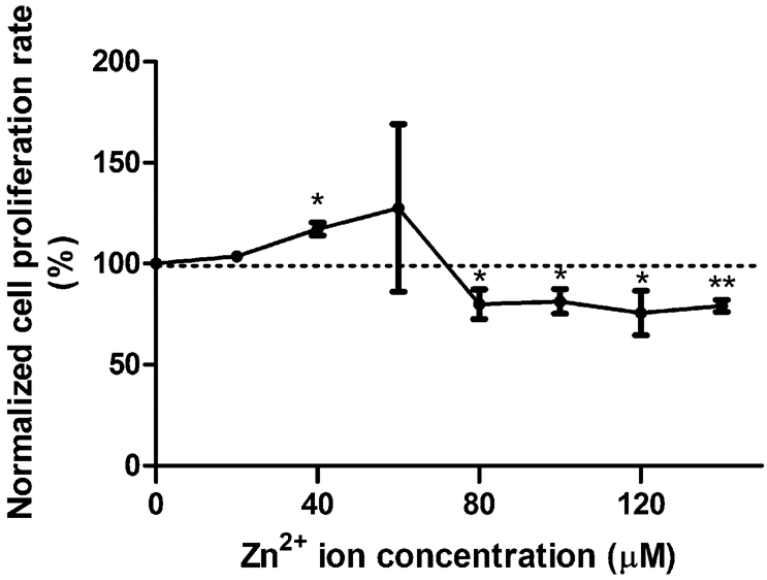

Figure 2.

BrdU cell proliferation assay. Cells were seeded and incubated for 24 h. Then, cells were treated with Zn^{2+} for 24 h. After that, cell proliferation was detected by a BrdU kit. Student's *t* test, * $p < 0.05$ and ** $p < 0.01$.

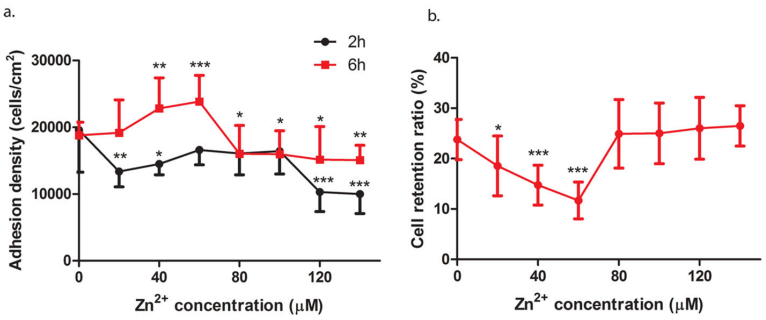

Figure 3.

Cell adhesion density and cell adhesion strength exposed to different concentrations of Zn^{2+}. (a) Cell adhesion test: ECs were mixed with Zn^{2+} solutions and allowed to attach for 2 and 6 h. (b) Cell adhesion strength test: ECs were mixed with Zn^{2+} solutions and allowed to attach for 6 h. After 6 h, the cell medium was replaced by DPBS. The plate were sealed and centrifuged at 500g for 5 min. Student's *t* test, * $p < 0.05$, ** $p < 0.01$, and *** $p < 0.001$.

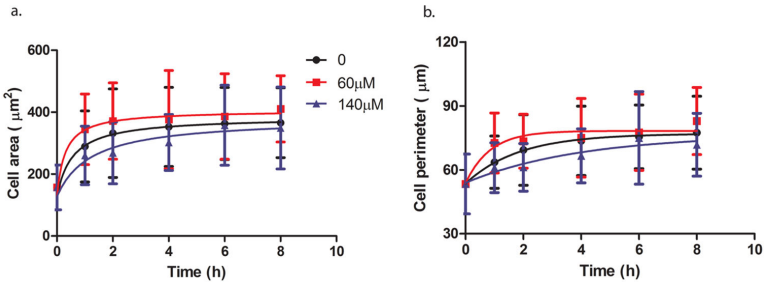

Figure 4.

Cell spreading at different concentrations of Zn^{2+}. (a) Cell area. (b) Cell perimeter. Cells were seeded with Zn^{2+} solutions, and at 0, 2, 4, 6, and 8 h, cells were stained by calcein AM. Cell area and perimeter were analyzed by ImageJ.

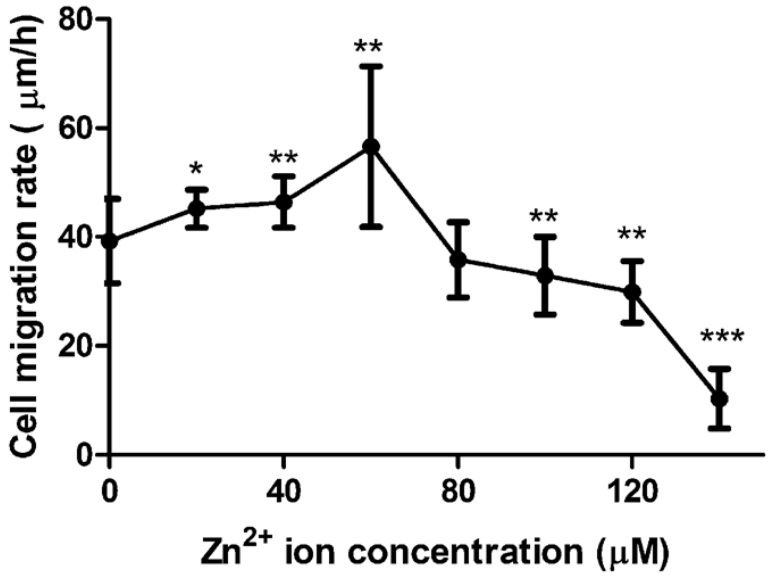

Figure 5.

Cell migration rate. Cells were seeded and incubated until a monolayer was formed. A p200 pipet tip was used to create the scratch. The width of the scratch was measured at 0 and 6 h. Student's *t* test, * $p < 0.05$, ** $p < 0.01$, and *** $p < 0.001$.

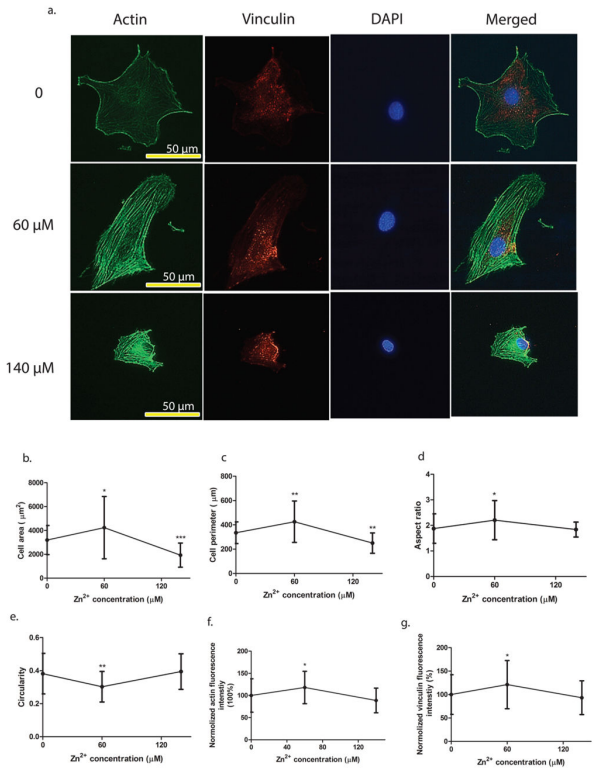

Figure 6.

Cytoskeletal reorganization and cell morphology characterization. (a) Representative images of immunofluorescence staining. (b) Cell area. (c) Cell perimeter. (d) Cell aspect ratio. (e) Cell circularity. (f) Normalized F-actin fluorescence intensity. (g) Normalized vinculin fluorescence intensity. Cells were seeded onto the cover glass and incubated for 24 h. Then, cells were fixed, permeabilized, and stained with different fluorescent colors for vinculin (red), actin (green), and nuclei (blue). The scale bar was 50 μm. Images were analyzed by ImageJ. Student's *t* test, * $p < 0.05$ and ** $p < 0.01$.

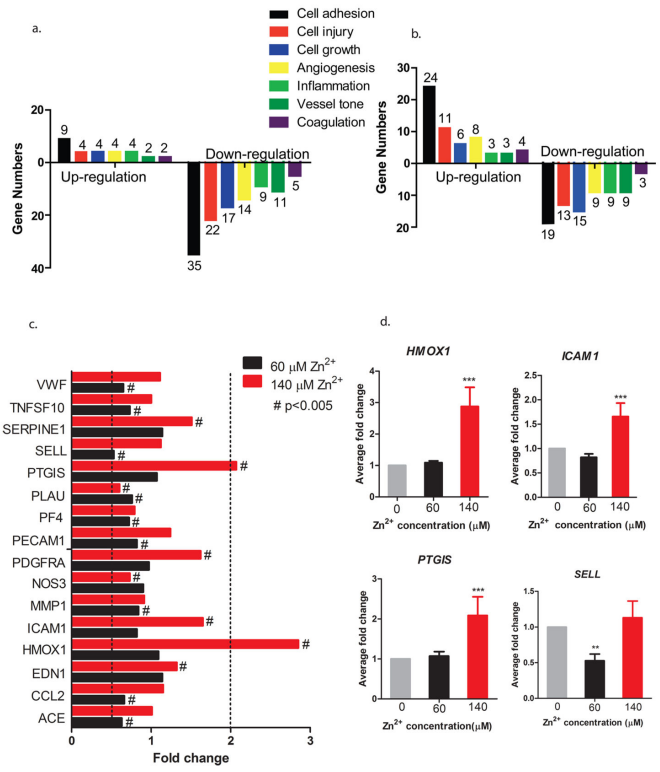

Figure 7.

Gene expression analysis of cells treated with Zn^{2+}. Cells were seeded in Petri dishes, and after a monolayer was formed, cells were treated with 60 μM or 140 μM Zn^{2+} for 24 h. After that, total RNA was isolated and reversely transcripted into cDNA, and RT-PCR was performed. (a) The number of affected genes by 60 μM Zn^{2+}. (b) The number of affected genes by 140 μM Zn^{2+}. (c) The significantly affected genes by Zn^{2+}. (d) The gene expression regulations of *HMOX1*, *ICAM1*, *PTGIS*, and *SELL*. Student's *t* test, # $p < 0.005$, ** $p < 0.01$, and *** $p < 0.001$.